Structural Dynamics in (ND$_4$)$_2$[Cu(D$_2$O)$_6$](SO$_4$)$_2$

Vanessa M. Masters and Mark J. Riley*

Department of Chemistry, University of Queensland, St Lucia, 4072, QLD, Australia

Michael A. Hitchman

Department of Chemistry, University of Tasmania, GPO Box 252-75, Hobart, 7001, TAS, Australia

The extended X-ray absorption fine structure spectroscopy (EXAFS) of (ND$_4$)$_2$[Cu(D$_2$O)$_6$](SO$_4$)$_2$ at 5, 14, 100, 200, and 298 K is reported. This indicates that the Cu−O bond lengths of the Cu(D$_2$O)$_6^{2+}$ ion do not change significantly within this temperature range, which contrasts with EPR results and X-ray and neutron diffraction experiments, which imply that two of the Cu−(D$_2$O) bonds converge in length as the temperature is raised. The EXAFS measurements thus confirm that the bond distances yielded by the diffraction experiments refer to the average positions of ligands involved in a dynamic equilibrium in which the directions of the long and intermediate bonds of the Jahn−Teller distorted Cu(D$_2$O)$_6^{2+}$ ion are interchanged in the crystal lattice. Analysis of the displacement parameters is consistent with this interpretation, as are the wave functions calculated using a model involving Jahn−Teller vibronic coupling and the influence of lattice strain interactions.

Introduction

In recent years there has been intense interest in the behavior of the deuterated ammonium copper Tutton salt (ND$_4$)$_2$[Cu(D$_2$O)$_6$](SO$_4$)$_2$. The directions of the long and intermediate axes of the distorted Cu(D$_2$O)$_6^{2+}$ octahedra interchange on deuteration, although the space group and C_i site symmetry of the copper(II) ion remains unaltered.[1] The (NH$_4$)$_2$[Cu(H$_2$O)$_6$](SO$_4$)$_2$ compound has its long axis along the Cu−O(7) bonds and has been designated as "type II", as shown in Figure 1. The deuterated compound, on the other hand, has its long axis along the Cu−O(8) bonds and is designated as "type I". The switch involves a large change in the bond lengths from (2.210 Å, 2.071 Å, 1.959 Å) to (2.078 Å, 2.222 Å, 1.960 Å) on deuteration at room temperature.[2] This very large isotopic effect can be viewed as a small perturbation magnified by the Jahn−Teller effect intrinsic to the Cu(D$_2$O)$_6^{2+}$ ion. It was subsequently found that the application of hydrostatic pressure switches the long axis of (ND$_4$)$_2$[Cu(D$_2$O)$_6$](SO$_4$)$_2$ from type I to type II.[3,4] This switch exhibits hysteresis at room temperature,[5] though the structure remains type II when the pressure is released below ∼290 K.[6]

Another interesting feature of the copper(II) Tutton salts is the observation that two of the molecular *g* values of the pure and magnetically dilute compounds[2,4,7−11] and Cu−O bond distances determined by neutron or X-ray diffraction[1,2] change
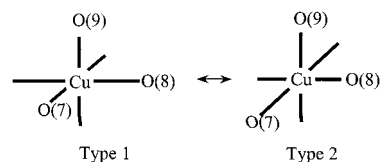

Figure 1. Type 1 and type 2 geometry for the Tutton salt systems. (ND$_4$)$_2$Cu(D$_2$O)$_6$(SO$_4$)$_2$ is type 1.

as a function of temperature. Initially, this observation was taken at face value; that is, it was assumed that the bond lengths and *g* values of the Cu(H$_2$O)$_6^{2+}$ ions simply alter as the temperature changes.[7] In a subsequent study, however, Silver and Getz proposed a different mechanism, hereafter referred to as the SG model.[9] In this model, the geometry and *g* values of the Cu(H$_2$O)$_6^{2+}$ ions themselves do not change with temperature, but each complex has two possible energy states with their long axes corresponding to type I or II packing in the crystal lattice. A thermal equilibrium is established between these forms, with the bond lengths and *g* values being averaged to reflect the position of this equilibrium. A more detailed approach was developed by Riley et al. (the RHW model).[10] This rationalizes the above observations in terms of a warped "Mexican hat" potential energy surface due to E⊗e Jahn−Teller coupling, modified by the low symmetry of the actual crystal site. Figure 2 shows the ^{2}E$_g$⊗e$_g$ ground state potential energy surface for an octahedral copper(II) complex as a function of the Jahn−Teller active e$_g$ coordinates. The atomic displacements of the two components of this doubly degenerate vibration, Q_θ, Q_ϵ, are also shown in Figure 2. The three equivalent minima in this potential energy surface correspond to linear combinations of Q_θ, Q_ϵ that give an octahedral geometry which is elongated

* Address correspondence to this author.
(1) Hathaway, B. J.; Hewat, A. W. *J. Solid State Chem.* **1984,** *51,* 364−375.
(2) Hitchman, M. A.; Maaskant, W.; van der Plas, J.; Simmons, C. J.; Stratemeier, H. *J. Am. Chem. Soc.* **1999,** *121,* 1488−1501.
(3) Simmons, C. J.; Hitchman, M. A.; Stratemeier, H.; Schultz, A. J. *J. Am. Chem. Soc.* **1993,** *115,* 11304−11311.
(4) Rauw, W.; Ahsbahs, H.; Hitchman, M. A.; Lukin, S.; Reinen, D.; Schultz, A. J.; Simmons, C. J.; Stratemeier, H. *J. Am. Chem. Soc.* **1996,** *35,* 1902−1911.
(5) Schultz, A. J.; Hitchman, M. A.; Jorgensen, J. D.; Lukin, S.; Radaelli, P. G.; Simmons, C. J.; Stratemeier, H. *Inorg. Chem.* **1997,** *36,* 3382−3385.
(6) Augustyniak, M. A.; Krupski, M.; *Chem. Phys. Lett.* **1999,** *311,* 126−130.
(7) Mabbs, F. E.; Porter, J. K. *J. Inorg. Nucl. Chem.* **1973,** *35,* 3219−3222.

(8) Duggan, M.; Murphy, A.; Hathaway, B. J. *Inorg. Nucl. Chem. Lett.* **1979,** *15,* 103−108.
(9) Silver, B. L.; Getz, G. *J. Chem. Phys.* **1974,** *61,* 638−650.
(10) Riley, M. J.; Hitchman, M. A.; Wan Mohammed, A. *J. Chem. Phys.* **1987,** *87,* 3766−3778.
(11) Ham, F. S. In *Electron Paramagnetic Resonance*; Geschwind, S., Ed.; Plenum: New York, 1972; pp 1−119.
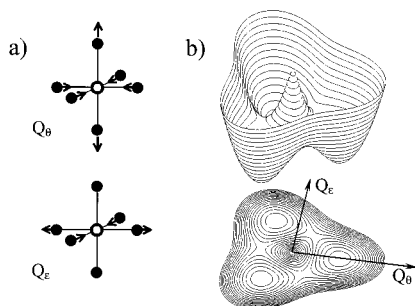
Figure 2. (a) The two components, Q_θ, Q_ϵ, of the Jahn−Teller active e_g vibration. (b) The lower part of the E⊗e potential energy surface, without low symmetry terms, as a function of Q_θ, Q_ϵ. The upper part of the conical intersection is not shown.

along the *x*, *y*, or *z* axes. In the solid state, a Jahn−Teller potential energy surface with strong coupling, as in the present case, is very sensitive to any low symmetry terms.[11]

The ground state potential energy surface for $Cu(D_2O)_6^{2+}$ in the $(ND_4)_2[Cu(D_2O)_6](SO_4)_2$ Tutton salt is dominated by a large negative tetragonal lattice strain interaction that opposes the inherent preference of $Cu(D_2O)_6^{2+}$ octahedra to be tetragonally elongated.[10] Together with a smaller orthorhombic low symmetry field, this results in three *inequivalent* minima, each of which corresponds closely to a tetragonal elongation of the octahedron along the different axes. For $(ND_4)_2[Cu(D_2O)_6]$-$(SO_4)_2$ it is the two lowest minima (separated by ∼300 cm^{-1}) that are the most important in determining the electronic and geometric properties of the compound. In a doped crystal where the $Cu(D_2O)_6^{2+}$ complex can be treated as an isolated ion, the properties displayed by the system are determined by a Boltzmann average of these two geometric isomers. In the case of pure copper(II) Tutton salts, deviations from this behavior occur which have been interpreted in terms of cooperative interactions.[2,12] These lead, in effect, to a temperature-dependent potential energy surface which causes deviations from the simple Boltzmann averaging of the bonds and *g* values of the two-level system.

In the model developed to describe the temperature dependence of the *g* values and bond distances of $(ND_4)_2[Cu(D_2O)_6]$-$(SO_4)_2$ observed by X-ray and neutron diffraction it was assumed that, although the cooperative interactions perturb the potential surface of the $Cu(D_2O)_6^{2+}$ ions at higher temperatures, this does not alter the Cu−O bond lengths, but simply changes the relative energy of the two structural isomers.[2] This somewhat surprising conclusion was rationalized in terms of the crystal packing, which means that when one complex switches from form I to II it is expected to alter the orthorhombic component but not the axial component of the lattice strain acting on its neighbors.[2] To test these assumptions, we have studied the extended X-ray absorption fine structure spectroscopy (EXAFS) of the compound over a temperature range. These results yield the *local* Cu−O bond distances and these are compared with those obtained from diffraction experiments and calculated vibronic wave functions. The anisotropic displacement parameters from the X-ray measurements contain additional useful information. If the change in bond lengths observed by X-ray diffraction is due to the weighted average of different Cu−O distances, this is expected to influence the anisotropy of the displacement parameters of the oxygen atoms, though no such effect was noted in the conventional analysis of the X-ray data.[2] Jahn−Teller distorted hydrates seem to be unusual in this respect,

since the displacement parameters of the oxygen atoms of the $Cr(H_2O)_6^{2+}$ ions in $[Cr(H_2O)_6]SiF_6$ also show no significant elongation along the Cr−O bond directions,[13] despite the fact that this complex is expected to show a Jahn−Teller distortion similar to its copper(II) analogue, with the long axis disordered equally along all three pairs of trans oxygen atoms. Indeed, this aspect was initially used as evidence that the Jahn−Teller distortion is quenched in this system,[13] though this conclusion was later modified.[14] To clarify this aspect, we analyze the displacement parameters from the X-ray measurements on $(ND_4)_2[Cu(D_2O)_6](SO_4)_2$ in terms of a simple two-level model and demonstrate that they are in fact consistent with a simple equilibrium of the SG type.

Experimental Section

Synthesis. The preparation of $(ND_4)_2[Cu(D_2O)_6](SO_4)_2$ has been described previously.[3]

EXAFS Measurements. X-ray absorption measurements were made at the Australian National Beamline Facility (ANBF) on bending-magnet beamline 20B at the KEK Photon Factory, Tsukuba, Japan. The sample was finely ground and diluted with boron nitride to give a 70% edge drop. Kapton Tape was used as windows to a 10 mm circular aperture in a 0.6 mm thick aluminum sample holder. At each temperature, two scans were collected and averaged over four stages: 8730−8930 eV (10 eV steps), 8930−9030(0.5) eV, 9030−9430(2.0) eV, 9430−10430(4.0) eV. Energies were calibrated using a Cu foil internal standard with the first inflection point of the K-edge being assigned as 8980.3 eV. The 2.5 GeV storage ring delivered a current of between 400 and 200 mA. The monochromator was a Si(III) channel cut double crystal detuned to 50% of the maximum intensity in order to reject higher harmonics. The data was collected in transmission mode using standard N_2-filled ionization chambers. The temperature of the sample was controlled by an Oxford instruments closed cycle cryostat.

The raw data was generally noise-free until $k \approx 12$. The scans were averaged based on signal-to-noise ratios. Background corrections were applied by fitting a polynomial and four-region spline to the preedge and EXAFS region, respectively. Data were normalized to an edge jump of 1 and $k = 0$ was calculated from $E_0 = 9000$ eV. The calculated EXAFS was fitted to the observed k^3 weighted data over the range 3(1)−12(1) Å^{-1}, with the *R* range from 1.2(0.5)−1.8(0.5) Å.

The EXAFS analysis was performed with the program suite XFIT[15] with FEFF 4.0[16] and FEFF 6.01[17] for single and multiple scattering, respectively. The goodness-of-fit is monitored by means of a residual, *R*, which can be calculated using

$$R = [\chi^2/\chi^2_{\text{calc}=0}]^{1/2} \tag{1}$$

where χ^2 is the quantity minimized in the refinement and $\chi^2_{\text{calc}=0}$ is the value of χ^2 when the calculated EXAFS is uniformly 0.

$$\chi^2 = \int_{k=0...\infty} [w(\chi_{\text{obs}}(k) - \chi_{\text{calc}}(k))]^2 \tag{2}$$

Here *w* is a weighting factor, $\chi_{\text{obs}}(k)$ is the observed and $\chi_{\text{calc}}(k)$ is the calculated EXAFS curve.

Computational Methods. We have used the basic E⊗e Jahn−Teller vibronic Hamiltonian with low-symmetry strain that has proved successful in interpreting the EPR of a series of copper(II) complexes.[2,3,10,18] This vibronic Hamiltonian includes first- and second-order coupling (A_1, A_2) and low-symmetry lattice strain terms (S_θ, S_ϵ)

(12) Henning, R. W.; Schultz, A. J.; Hitchman, M. A.; Kelly, G.; Astley, T. *Inorg. Chem.* **2000**, *39*, 765−769.

(13) Cotton, F. A.; Falvello, L. R.; Murillo, C. A.; Quesada, J. F. *J. Solid State Chem.* **1992**, *96*, 192−198.

(14) Falvello, L. R. *J. Chem. Soc., Dalton Trans.* **1997**, 4463−4475.

(15) Ellis, P. J.; Freeman, H. C. *J. Synchrotron Radiat.* **1995**, *2*, 190−195.

(16) Rehr, J. J.; Mustre de Leon, J.; Zabinsky, S. I.; Albers, R. C. *J. Am. Chem. Soc.* **1991**, *113*, 5135−5140.

(17) Mustre de Leon, J., Rehr, J. J., Zabinsky, S. I. and Albers, R. C. *Phys. Rev. B* **1991**, *44*, 4146−4156.

(18) Bebendorf, J.; Bürgi, H.-B.; Gamp, E.; Hitchman, M. A.; Murphy, A.; Reinen D.; Riley, M. J.; Stratemeier, H. *Inorg. Chem.* **1996**, *35*, 7419−7429.
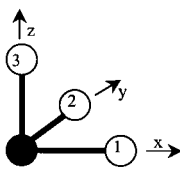
as described previously. The D_2O ligand is treated as a point mass of 20 amu for the "reduced mass" of the Jahn−Teller active e_g vibration.[19] Here we briefly outline the methods used to calculate the geometric properties from the resulting vibronic wave functions.

A total vibronic basis size of 2862 was used, which cannot be factored into symmetry blocks due to the S_θ, S_ϵ low-symmetry terms. The vibronic eigenfunctions of the Hamiltonian, Ψ, were found in terms of the basis functions, which consist of a triple product of one electronic, ψ, and two vibrational, ϕ, states.

$$\Psi = \sum_{l=\theta,\epsilon} \sum_{i+j=0}^{n_e} a_{lij} \psi_l \phi_i \phi_j \qquad (3)$$

The electronic states ψ_θ, ψ_ϵ are the two components of the orbital part of the ^2E_g electronic ground state of the hypothetical octahedral copper(II) complex; $\phi_i \phi_j$ are the one-dimensional harmonic oscillator basis functions of the octahedral e_g vibration.

The mean and mean-squared bond lengths can be directly calculated from the vibronic wave functions. The values $\langle x_1 \rangle$, $\langle y_2 \rangle$, $\langle z_3 \rangle$ refer to the x, y, and z relative displacements of the ligands 1, 2, 3 from the $Q_\theta = Q_\epsilon = 0$ octahedral geometry.

$$\langle x_1 \rangle = -\sqrt{\frac{1}{12}}\langle Q_\theta \rangle + \frac{1}{2}\langle Q_\epsilon \rangle$$

$$\langle y_2 \rangle = -\sqrt{\frac{1}{12}}\langle Q_\theta \rangle - \frac{1}{2}\langle Q_\epsilon \rangle \qquad (4a)$$

$$\langle z_3 \rangle = \sqrt{\frac{1}{3}}\langle Q_\theta \rangle$$

$$\langle x_1^2 \rangle = \frac{1}{12}\langle Q_\theta^2 \rangle - \frac{1}{2\sqrt{3}}\langle Q_\theta Q_\epsilon \rangle + \frac{1}{4}\langle Q_\epsilon^2 \rangle$$

$$\langle y_2^2 \rangle = \frac{1}{12}\langle Q_\theta^2 \rangle + \frac{1}{2\sqrt{3}}\langle Q_\theta Q_\epsilon \rangle + \frac{1}{4}\langle Q_\epsilon^2 \rangle \qquad (4b)$$

$$\langle z_3^2 \rangle = \frac{1}{3}\langle Q_\theta^2 \rangle$$

The mean-squared displacements can be related to the thermal displacement parameters in the metal−ligand direction[19] whereas cross terms such as $\langle x_1 y_2 \rangle$ are the mean-squared quantities between different atoms, and will not concern us here. The quantities $\langle Q_\theta \rangle$, $\langle Q_\epsilon \rangle$, $\langle Q_\theta^2 \rangle$, $\langle Q_\theta Q_\epsilon \rangle$, and $\langle Q_\epsilon^2 \rangle$ in eq 4 can be calculated by using the matrix elements of the simple harmonic oscillator functions,[18] and an example of the calculation of $\langle Q_\theta \rangle$ is shown below.

$$\langle Q_\theta \rangle = \langle \Psi | Q_\theta | \Psi \rangle$$

$$= \sum_{l=\theta,\epsilon} \sum_{i+j=0}^{n_e} \sum_{i'+j'=0}^{n_e} a_{lij} a_{li'j'} \langle \phi_i | Q_\theta | \phi_{i'} \rangle \langle \phi_j | \phi_{j'} \rangle$$

$$= \sum_{l=\theta,\epsilon} \sum_{i+j=0}^{n_e} a_{lij} a_{li-1j}\sqrt{\frac{i}{2}} + a_{lij}a_{li+1j}\sqrt{\frac{i+1}{2}} \qquad (5)$$

The mean and mean-squared displacements of eq 4 represent the first two moments in the probability distribution, the explicit form of which can also be calculated. The probability distributions as a function of x_1, y_2, and z_3 can be found by stepping through the linear combinations of Q_θ, Q_ϵ in eq 4a and integrating over the three-dimensional vibronic function in the directions perpendicular to this. As an example, Figure 3a shows the probability function for the lowest calculated vibronic level in the absence of the S_θ, S_ϵ low-symmetry terms and with linear coupling only. The upper part of the figure shows the vibronic probability as a function of the Q_θ, Q_ϵ coordinates. Below this is the
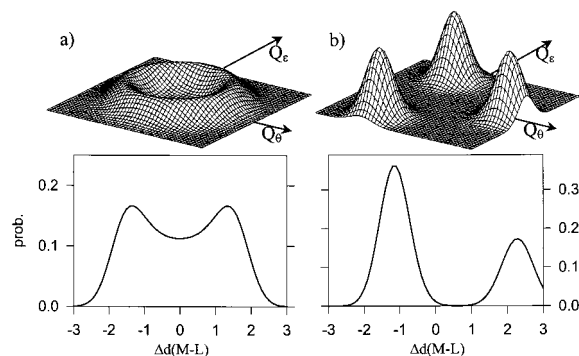
(19) Cyvin, S. J. *Molecular Vibrations and Mean Squared Amplitudes*; Elsevier: Amsterdam, 1968.

Figure 3. Calculated probability function for the lowest vibronic state in an ML_6 $E \otimes e$ system. The probability is a function of Q_θ, Q_ϵ in the upper figure and as a displacement of the metal−ligand bond lengths from their equilibrium values. This latter function is identical for all six ligands. (a) First-order Jahn−Teller coupling, $A_1/h\nu = 3.0$, $A_2/h\nu = 0.0$ (b) Second-order Jahn−Teller coupling, $A_1/h\nu = 3.0$, $A_2/h\nu = 0.125$.
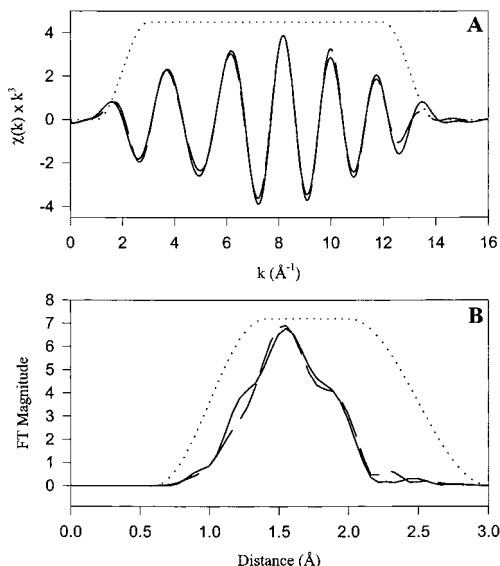

Figure 4. (A) The filtered EXAFS (B) Fourier transform amplitude of the EXAFS for $(ND_4)_2[Cu(D_2O)_6](SO_4)_2$ at 14 K. Observed (—), calculated from refined model (− − −), window used in Fourier filter (···).

vibronic probability as a function of the displacements from the mean position, x_1, y_2, or z_3, all of which are equal in this case. In the absence of low-symmetry terms, the *mean* geometry of a Jahn−Teller system is the high-symmetry undistorted geometry. In Figure 3a the first-order coupling calculation shows a probability function with two *equal* maxima. If the other sources of mean-squared motion were absent, the probability density function of all ligands of this system would resemble dumbbells rather than ellipsoids, symmetric about the undistorted geometry.

Figure 3b shows a calculation with both first- and second-order coupling. In this case, the probability density function of all ligands would resemble asymmetric dumbbells. The probability distribution reflects what is expected for an elongated octahedral geometry at the minima of the warped Jahn−Teller potential surface. However, the distortion is dynamic, not static. Each ligand will have a two-thirds probability of being displaced less than the equilibrium bond length and one-third probability of being displaced further than the equilibrium bond length by twice this amount.

Results

EXAFS Experiments. The EXAFS of $(ND_4)_2[Cu(D_2O)_6]-(SO_4)_2$ were measured at the temperatures 14, 100, 200, and 298 K. The filtered EXAFS and its Fourier transform amplitude at a temperature of 14 K are shown in Figure 4 together with

Table 1. Structural Parameters for the $Cu(D_2O)_6^{2+}$ Ion in $(ND_4)_2[Cu(D_2O)_6](SO_4)_2$ from the EXAFS Analysis Compared with Crystal Structure Data at 5 K

	crystal struct[1] 5 K	EXAFS model 14 K	EXAFS model 100 K	EXAFS model 200 K	EXAFS model 298 K
Cu−O7 (Å)	2.011(4)	2.01(1)	2.00(1)	2.01(1)	2.01(3)
Cu−O8 (Å)	2.304(6)	2.29(2)	2.28(3)	2.30(1)	2.29(2)
Cu−O9 (Å)	1.951(4)	1.95(1)	1.95(1)	1.95(1)	1.95(1)
O7−Cu−O8 (deg)	87.2(2)	89.5	87.2	90.2	87.2
O8−Cu−O9 (deg)	88.8(2)	89.8	88.8	90.2	88.8
O9−Cu−O7 (deg)	90.2(2)	92.5	90.2	88.8	90.2
E_0 (eV)		8991(1)	8992(2)	8991(1)	8990(1)
S_0^2		0.86(5)	0.81(9)	1.0(1)	1.0(1)
R value		0.129	0.129	0.141	0.149
σ(Cu−O7)		0.0034(20)	0.0011(10)	0.0080(30)	0.0069(10)
σ(Cu−O8)		0.0038(20)	0.0035(10)	0.0080(10)	0.0127(80)
σ(Cu−O9)		0.0034(20)	0.0036(20)	0.0041(5)	0.0038(10)

the fitted calculated spectrum. Using only the first coordination shell and single scattering theory, several models were investigated using the FEFF4 program.[16] These included octahedral and varying degrees of tetragonal and rhombic distortion. The models for a tetragonal distortion included both compression and elongation. After preliminary results (at all temperatures) indicated that the copper center was in an environment with four short and two long bonds, suitable models were refined using multiscattering theory.[17]

For the 14 K data, the initial EXAFS model was based on the crystal structure at 5 K.[1] Attempts were made to fit the EXAFS spectra at 100, 200, and 298 K with models based upon relevant higher temperature crystal structure geometry. However, the fits resulting from these models were quite poor (R values 24−50%). When the bond lengths/angles were allowed to vary, the resultant structure refined to have a geometry similar to the crystal structure at 5 K. During the refinement process, the threshold energy (E_0), as well as the positions and Debye−Waller factors (σ^2) of all the atoms in the model and the amplitude scale factor (S_0^2), was treated as variables while the coordination number (N) was kept constant. The calculations included 14 unique paths with an effective length <4 Å and up to four legs. The goodness-of-fit parameter, R, was calculated using eq 1 and the final R values are given in Table 1.

The standard deviations were estimated using two methods. The first method uses XFIT[15] to fit a series of EXAFS curves generated by adding random noise at the same level found in the original EXAFS to the original EXAFS curve that had been smoothed. The noise in the observed EXAFS was then estimated using Fourier filtering. The second method extracted several EXAFS spectra using slightly different spline curves. These EXAFS spectra were then modeled using the same methods as the initial EXAFS spectrum and the standard deviations were estimated from the range of values obtained.

Anisotropic Displacement Parameters. The difference in vibrational parameters ΔU evaluated along bonded atoms contains information on the internal molecular motion. This has been previously studied for both molecules with small- and large-amplitude motions.[20] Examples of large-amplitude motion in metal complexes that have previously been analyzed include spin equilibrium in Fe(III) complexes[21] and pseudo Jahn−Teller *cis*- $Cu^{(II)}N_4O_2$ systems.[22] The latter case is very similar to the present system, as the cis coordination causes the two axial N ligands to form stronger bonds than the equatorial O/N pairs. This results in an effective tetragonal compression being added

to the basic octahedral ligand field. Together with a small orthorhombic low-symmetry component, this produces two inequivalent minima close in energy, with the long axes interchanged as shown for the present compound in Figure 1.

It has been noted for $(ND_4)_2[Cu(D_2O)_6](SO_4)_2$ that the anisotropic displacement parameters of the water oxygen atoms are not unusually large.[1,2] In particular, the displacement parameters of the oxygen atoms (O7, O8) in $(ND_4)_2[Cu(D_2O)_6]$-$(SO_4)_2$ are not elongated appreciably in the Cu−O bond direction as might be expected for an averaged structure of two isomers with different bond lengths. However, it will be shown that the ΔU's are much more sensitive to this averaging than the U's.

Using a procedure described previously,[22,24] the difference in the mean-square displacements along the copper−oxygen bonds was extracted from the anisotropic displacement parameters. The mean square displacement $\langle u^2 \rangle$ in a particular direction (i.e., along a metal−ligand bond) can be calculated using $\langle u^2 \rangle = \mathbf{I}^T U \mathbf{I}$, where $\mathbf{I}$ is a unit vector in the desired direction and the 3 × 3 matrix and U is the anisotropic displacement parameters represented in a Cartesian coordinate system. If one is determining the difference in mean square displacement in a specific direction such as along a M−L bond, then

$$\Delta U = \mathbf{I}^T \mathbf{U}(L)\mathbf{I} - \mathbf{I}^T \mathbf{U}(M)\mathbf{I} \qquad (6)$$

where $\mathbf{U}(L)$ and $\mathbf{U}(M)$ are the anisotropic displacement matrices of a ligating atom and the metal atom, respectively, and the direction of the unit vector is along the metal−ligand bond. The ΔU's can be calculated in a two-level model by summing the contribution from the bond stretching motions and the contribution due to the static Jahn−Teller distortions. These two terms represent respectively the contribution from the ΔU's from *within* each level and the contributions from the *difference* in the bond lengths of the two levels.

Assuming the simple two-level model where the upper level has the same bond lengths as the lower level with the long and intermediate bonds (and their displacement amplitudes ΔU_l and ΔU_s respectively) interchanged, one then finds that ΔU_{obs} for both Cu−O7 and Cu−O8 is given by the following.

$$\Delta U_{obs} = a_0 + a_1\langle\Delta d(Cu-O)\rangle - \langle\Delta d(Cu-O)\rangle^2$$

$$a_0 = (\Delta U_l + \Delta U_s)/2 + (\Delta d(Cu-O))^2$$

$$a_1 = (\Delta U_l - \Delta U_s)/2/\Delta d(Cu-O) \qquad (7)$$

(20) Trueblood, K. N.; Dunitz, J. D. *Acta Crystallogr. B* **1983**, *39*, 120−133.
(21) Chandrasekhar, K.; Bürgi, H.-B. *Acta Crystallogr. B* **1984**, *40*, 387−397.
(22) Stebler, M.; Bürgi, H.-B. *J. Am. Chem. Soc.* **1987**, *109*, 1395−1401.
(23) Simmons, C.; Hitchman, M. A.; Stratemeier, H.; Astley, T. *Inorg. Chem.* **2000**, *39*, 4651−4653.
(24) Dunitz, J. D. *X-ray Analysis and Structure of Organic Molecules*; Verlag Helvetica Acta: Basel, Switzerland, 1995.
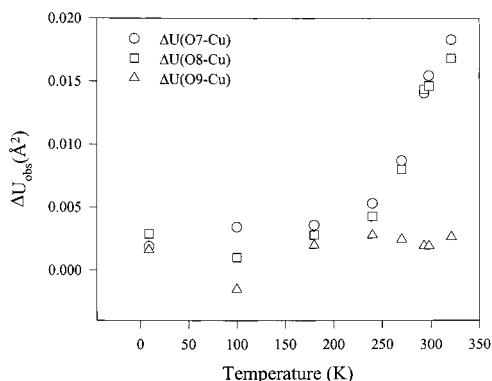
Figure 5. Mean square displacement, ΔU_{obs} (Å^2), along the copper−oxygen bonds for (ND$_4$)$_2$[Cu(D$_2$O)$_6$](SO$_4$)$_2$. Data from 9 K;[29] 293 K;[31] 100, 180, 240, 298, 321 K[2].
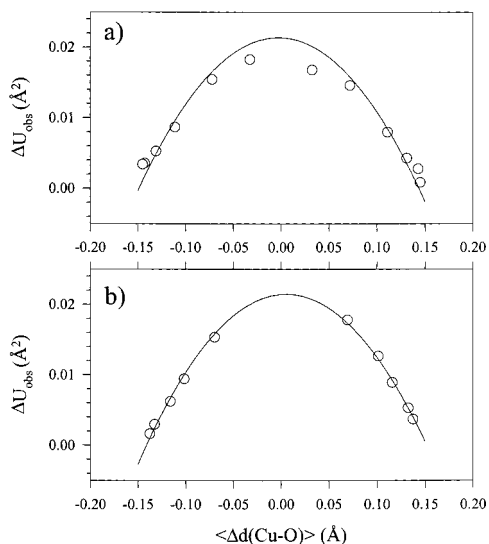
Figure 6. Scatter plot of ΔU_{obs}(Cu−O) (Å^2) vs $\langle \Delta d$(Cu−O)$\rangle$ (Å) for (a) (ND$_4$)$_2$[Cu(D$_2$O)$_6$](SO$_4$)$_2$ and (b) (NH$_4$)$_2$[Cu(H$_2$O)$_6$](SO$_4$)$_2$. Calculated using data from ref 2. The solid line represents the quadratic fit.

Here Δd(Cu−O) $\equiv$ [d(Cu−O′) − d(Cu−O″)]/2, half the difference in the *actual* bond length of the lower (′) and upper (″) levels and $\langle \Delta d$(Cu−O)$\rangle \equiv$ [$\langle d$(Cu−O7)$\rangle - \langle d$(Cu−O8)$\rangle$]/2, is half the difference in the *observed* bond lengths. From this equation, it is expected that there will be a quadratic dependence of the displacement amplitudes, ΔU_{obs}, on half the difference in the *observed* bond lengths, $\langle \Delta d$(Cu−O)$\rangle$.

The anisotropic displacement parameters for (ND$_4$)$_2$[Cu-(D$_2$O)$_6$](SO$_4$)$_2$ and (NH$_4$)$_2$[Cu(H$_2$O)$_6$](SO$_4$)$_2$ have previously been determined[2] and are given as Supporting Information to ref 2. The differences between the displacement parameters along the Cu−O bonds are shown as a function of temperature as the symbols in Figure 5. These values of ΔU are very similar at low temperature and remain relatively constant for the shortest Cu−O9 bond. The ΔU values for the other two bonds show a marked temperature dependence, increasing to 0.018 Å^2 at 321 K. This value is an order of magnitude larger than the ∼0.002−0.003 Å^2 usually seen, for example, in the internal stretching vibrations of complexes such as Ni(NH$_3$)$_6^{2+}$ [21] or (ND$_4$)$_2$[Zn-(D$_2$O)$_6$](SO$_4$)$_2$.[23]

The ΔU_{obs} values are plotted against $\langle \Delta d$(Cu−O)$\rangle$ in Figure 6 for both (ND$_4$)$_2$[Cu(D$_2$O)$_6$](SO$_4$)$_2$ and (NH$_4$)$_2$[Cu(H$_2$O)$_6$]-(SO$_4$)$_2$. Both the deuterated and nondeuterated compounds show very good agreement with the predicted quadratic dependence. The fitted solid line gives values of $a_0 = 0.0214$ Å^2, $a_1 =$

Table 2. Difference in the Mean Square Displacement Parameters (Å^2) for (ND$_4$)$_2$[Cu(D$_2$O)$_6$](SO$_4$)$_2$ and (NH$_4$)$_2$[Cu(H$_2$O)$_6$](SO$_4$)$_2$

temp (K)	ΔU_{obs}(Cu−O7)	ΔU_{obs}(Cu−O8)	ΔU_{dis}(calc)^a	ΔU_{obs}(calc)^a
	(ND$_4$)$_2$[Cu(D$_2$O)$_6$](SO$_4$)$_2$			
321	0.018	0.017	0.018	0.020
298	0.015	0.015	0.014	0.016
270	0.009	0.008	0.007	0.009
240	0.005	0.004	0.002	0.004
180	0.004	0.003	−0.001	0.001
100	0.003	0.001	−0.0016	0.0004
	(NH$_4$)$_2$[Cu(H$_2$O)$_6$](SO$_4$)$_2$			
298	0.018	0.015	0.015	0.017
270	0.013	0.009	0.009	0.011
240	0.009	0.006	0.006	0.008
180	0.005	0.003	0.002	0.004
100	0.004	0.002	0.000	0.002

^{a} ΔU_{dis} and ΔU_{obs} are calculated assuming $\Delta U_l = \Delta U_s = 0.002$ Å^2 and $\langle \Delta d$(Cu−O)$\rangle = 0.1356$ Å, see text.

−0.0052 Å, and $a_0 =$0.0214 Å^2, $a_1 = 0.0108$ Å for the D(H) compounds, respectively. Table 2 gives the ΔU_{obs} at the different temperatures. We now investigate the different contributions to these values. From Figure 5 one sees that the *observed* values ΔU_{obs}(Cu−O7) and ΔU_{obs}(Cu−O8) are close and if one assumes that the *actual* values are equal $\Delta U_l = \Delta U_s = \Delta U$, then $a_1 = 0$ and $a_0 = \Delta U + (\Delta d$(Cu−O))^2 in eq 7. One can estimate ΔU from the temperature-independent ΔU(Cu−O9) as ∼0.002 Å^2 and use the a_0 determined in Figure 6 to find an accurate value of Δd(Cu−O). One finds for both the deuterated and nondeuterated compounds that Δd(Cu−O) = 0.1393 Å. The last two columns of Table 2 show the calculated ΔU_{obs} from the fitted curve at the appropriate observed $\langle \Delta d$(Cu−O)$\rangle$ values, and the contribution to this from ΔU_{dis}. It can be seen that at temperatures >200 K ΔU_{dis} makes the dominant contribution.

These temperature-independent coefficients a_0 and a_1 could in principle also be calculated from the low-temperature bond lengths d(Cu−O7), d(Cu−O8) and differences in displacement parameters ΔU(Cu−O7) and ΔU(Cu−O8). While the relationship between ΔU and $\langle \Delta d \rangle$ can be determined by the low-temperature values, the fit of the parabola to the data of many different temperatures in Figure 6 is far more accurate. It also demonstrates that at all temperatures the averaging of the bond lengths is indeed due to a thermal equilibrium as assumed by the two-level model. Equation 7 is not obeyed when the averaging of structural isomers is not in thermal equilibrium as is the case for static rather than dynamic disorder.[22]

Model Calculation. The following set of parameters was used to calculate the geometric properties of the individual vibronic states of the Cu(D$_2$O)$_6$ ion in (ND$_4$)$_2$[Cu(D$_2$O)$_6$](SO$_4$)$_2$ and thereby the temperature dependence of the geometry of this complex (cooperative interactions are ignored here,[2] but the results should be accurate enough for the present purposes).

$$h\nu = 300 \text{ cm}^{-1}, \quad A_1 = 1100 \text{ cm}^{-1}, \quad A_2 = 33 \text{ cm}^{-1},$$
$$S_\theta = -600 \text{ cm}^{-1}, \quad S_\epsilon = -200 \text{ cm}^{-1} \quad (8)$$

These parameters are similar to those derived from the analysis of the temperature dependence of the bond distances of the compound.[3] Similar values were found[3] for (NH$_4$)$_2$[Cu-(H$_2$O)$_6$](SO$_4$)$_2$ and copper(II)-doped (ND$_4$)$_2$[Zn(D$_2$O)$_6$](SO$_4$)$_2$,[2] except for the negative sign of S_ϵ. The potential surface obtained from these parameters has three inequivalent minima. The lowest vibronic wave functions are localized within these minima though higher wave functions can be delocalized over two or

Table 3. Calculated Vibronic Energy Levels and Geometric Properties for $(ND_4)_2[Cu(D_2O)_6](SO_4)_2{}^a$

energy (cm^{-1})	$d(Cu-O7)$ (Å)	$d(Cu-O8)$ (Å)	$d(Cu-O9)$ (Å)	$\langle\Delta d(Cu-O7)^2\rangle$ (Å^2)	$\langle\Delta d(Cu-O8)^2\rangle$ (Å^2)	$\langle\Delta d(Cu-O9)^2\rangle$ (Å^2)
0.0	2.0028	2.3112	1.9860	0.0012	0.0012	0.0011
249.8	2.0096	2.3071	1.9834	0.0031	0.0032	0.0011
286.5	2.0015	2.3088	1.9897	0.0018	0.0017	0.0033
316.4	2.3080	2.0100	1.9820	0.0013	0.0013	0.0011
486.8	2.0230	2.2971	1.9800	0.0058	0.0052	0.0011
538.1	2.0065	2.3062	1.9873	0.0033	0.0044	0.0033
547.6	2.2961	2.0254	1.9785	0.0038	0.0042	0.0011
568.4	2.0009	2.3051	1.9940	0.0026	0.0021	0.0055
607.7	2.3070	2.0075	1.9855	0.0020	0.0017	0.0032
692.4	2.0813	2.2438	1.9749	0.0136	0.0122	0.0011

^{a} The parameters listed in eq 8 were used. Note that the mean-squared values are calculated from eq 4 with respect to the octahedral geometry. This is converted to dimensioned coordinates[18] with respect to the mean geometry of each level.

more minima. The extent of delocalization increases at energies around and above the barrier height between the minima. The electronic and geometric properties at a particular temperature will be a Boltzmann average of properties of the individual vibronic levels as long as the exchange between the levels is fast on the time scale of the experiment used to measure the properties, as is the case for EPR, or is a space-averaged property, as occurs for X-ray and neutron diffraction experiments. However, EXAFS measurements yield the *local* Cu−O bond lengths. It is noted that the rate of relaxation between the vibronic levels is also determined by the "overlap" of vibronic levels as well as their fractional populations. The exchange between vibronic levels that are localized within different minima often proceeds faster via a vibronic level that is delocalized over both minima, rather than by a direct process.[25]

The energy levels and geometric properties of the 10 lowest vibronic wave functions are given in Table 3. Here it is seen that the fourth level is localized in the upper minimum, having similar bond lengths to the lowest level but with the long and intermediate bonds interchanged. The energy difference ∼315 cm^{-1} will be the important energy for establishing the Boltzmann averaging of properties, though the vibronic levels at 250 and 285 cm^{-1} may be important as an pathway between the two mimina. The mean-squared bond lengths increase for the higher levels as the vibronic wave functions become more delocalized.

This is shown explicitly in Figure 7 where the probability distribution is shown along $x(Cu-O7)$, $y(Cu-O8)$, and $z(Cu-O9)$ axes for the four lowest energy vibronic wave functions. These probability amplitudes for levels 1−4 are given as solid, long dash, short dash, and dotted lines, respectively, and have been multiplied by a Boltzmann factor to show their relative contributions at 300 K. Clearly the lowest level (solid line) is elongated along the $y(Cu-O8)$ axis as in the low-temperature crystal structure, while the fourth level (dotted line) is an elongation along $x(Cu-O7)$ and is localized in the upper minimum.

Discussion

At low temperature, the neutron[1] and X-ray[2] crystal structure determinations of $(ND_4)_2[Cu(D_2O)_6](SO_4)_2$ show that the copper(II) center exists in an elongated octahedral geometry, with a rhombic distortion. As the temperature is increased the Cu−O(8) bond distance decreases, while the Cu−O(7) bond increases and the Cu−O(9) distance remains essentially constant. At 321 K the structure appears to approach a tetragonally compressed geometry.[2]
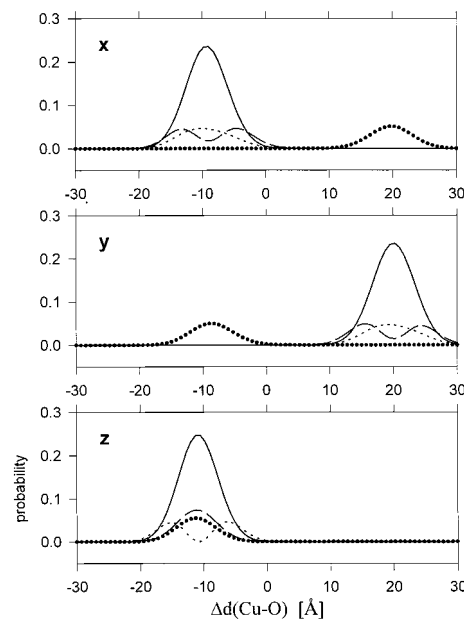
(25) Yablokov, Yu. V.; Hitchman, M. A.; Riley, M. J.; Stratemeier, H., to be published.

Figure 7. Probability distribution of the vibronic wave functions along the $x(Cu-O7)$, $y(Cu-O8)$, and $z(Cu-O9)$ bonds relative to the mean bond length of 2.09 Å at low temperature. The solid, large dash, small dash, and dotted lines are the calculated vibronic levels at 0, 250, 287, and 316 cm^{-1}, respectively. The amplitude has been multiplied by a Boltzmann factor for a temperature of 300 K.

The EXAFS of $(ND_4)_2[Cu(D_2O)_6](SO_4)_2$ at the four different temperatures superficially looks very similar, although there is some broadening and smoothing with increasing temperature. Qualitatively this indicates that the local copper(II) geometry remains unchanged as the temperature is varied, and the final fitted models given in Table 1 show that the Cu−O bond lengths are essentially temperature independent. For the most part, the Debye−Waller factors follow the pattern $\sigma(Cu-O8) > \sigma(Cu-O7) > \sigma(Cu-O9)$, as expected from the variation in bond lengths $d(Cu-O8) > d(Cu-O7) > d(Cu-O9)$ and the averaging processes discussed above. The values for E_0 and $S_0{}^2$ should be approximately the same for all models at the different temperatures. If both are allowed to vary, they refine to slightly different values. If E_0 and $S_0{}^2$ were fixed at the value found for the 14 K structure, it was found that there was little difference in the resulting R value for the higher temperature data sets.

The copper−oxygen bond lengths as determined by EXAFS are compared with the values obtained using diffraction techniques in Figure 8. The temperature dependence of the EXAFS of $(ND_4)_2[Cu(D_2O)_6](SO_4)_2$ shows that as the temperature is increased, there is no significant change in the local copper−oxygen bond lengths. Though the value calculated from
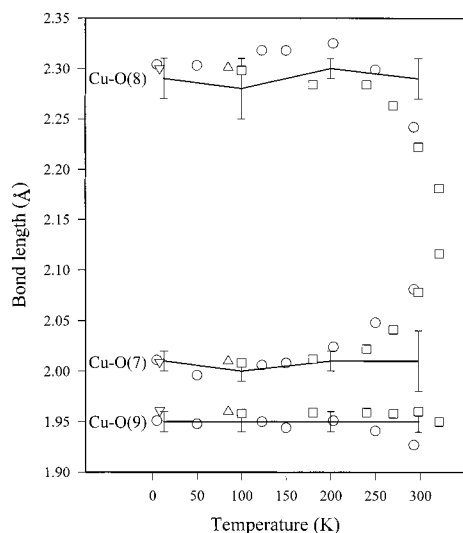
Figure 8. Cu—O bond lengths of (ND$_4$)$_2$[Cu(D$_2$O)$_6$](SO$_4$)$_2$ as a function of temperature from X-ray diffraction (data from circles;[1] triangles down;[29] squares;[2] triangles[30]) and from fitting the EXAFS spectra (solid lines). The error bars in the EXAFS are discussed in the text.

the EXAFS for the longest Cu—O bond length is slightly less than that observed in the low-temperature crystal structure it has been noted previously,[26,27] from the EXAFS of aqueous Cu-(H$_2$O)$_6^{2+}$ that the four shorter bonds dominate the scattering, making the determination of the longer bonds less reliable. This means that the *superposition* of the bond lengths for each vibronic level that is thermally populated, weighted by its occupation, is not expected to change significantly between 5 and 320 K.

This is again shown explicitly in the calculated probability distributions shown in Figure 7. In an X-ray structural determination the atomic positions are determined as mean values. The mean values of x(Cu—O7) and y(Cu—O8) will gradually approach each other as the temperature is increased, while z(Cu—O9) will be temperature independent. This is what is observed experimentally as shown as symbols in Figure 8. However, the mean value of the probability distribution for *each* vibronic state in Figure 7 is all localized in one of two positions for x(Cu—O7) and y(Cu—O8); and localized about a single value for z(Cu—O9). The EXAFS measures the radial probability distribution of all bonded atoms which corresponds to the superposition of x, y, and z. As implied by the calculations in Figure 7 and the experimental EXAFS (lines in Figure 8), this results in the temperature-independent four short and two long bonds of a tetragonally elongated octahedron. This is instead of the gradual averaging of the x(Cu—O7) and y(Cu—O8) bonds implied by the X-ray crystallography.

The results thus confirm that the SG and RHW models are good approximations for the basic behavior of (ND$_4$)$_2$[Cu(D$_2$O)$_6$]-(SO$_4$)$_2$ and that the change in g values and bond distances observed in the diffraction experiments is due to a thermal equilibrium involving vibronic wave functions which are localized, and correspond to complexes with similar bond lengths but different orientations in the crystal lattice. Because the EXAFS suggests there is no significant change in the copper—oxygen bond lengths as the temperature is increased,

this confirms the conclusion[2] that the cooperative interactions in the crystal do not perturb the local geometry of the Cu(H$_2$O)$_6^{2+}$, but simply influence the relative energies of the structural isomers.

As in previous studies,[22] it should be noted that the agreement of the observed difference displacement parameters (ΔU's) with eq 7, as shown in Figure 6, is much better than might be anticipated. This is thought to be due to the fact that systematic errors, for example from incorrect absorption corrections, tend to cancel in the calculation of the ΔU's. In other words, the ΔU's contain more reliable physical information than the U's themselves. It has also been pointed out that agreement between the observed and calculated ΔU's is not correlated with the accuracy of the structure determination.[22] The excellent agreement shown in Figure 6 confirms that the X-ray scattering is produced by the superposition of the vibronic wave functions localized at each minimum. This is in contrast to the EXAFS measurements, where the interaction is due to the local environment of the copper

A remaining point is the reason for the switch from structure type II to type I on deuteration. The isotope-induced phase transition of (NH$_4$)$_2$[Cu(H$_2$O)$_6$](SO$_4$)$_2$ does not occur if H$_2^{18}$O is substituted instead of D$_2$O.[28] This implies that the geometry change on deuteration is not simply due to the mass change of the ligand, but rather perhaps to the effect that deuteration has on the hydrogen bonding in this compound.

Conclusions

The EXAFS spectrum of (ND$_4$)$_2$[Cu(D$_2$O)$_6$](SO$_4$)$_2$ over a temperature range indicates that the gradual change in bond distance seen in the neutron and X-ray diffraction structure determinations is due to a dynamic averaging of two structural isomers. This is in agreement with previous interpretations of both X-ray diffraction and EPR experiments and also with the calculated vibronic wave functions of the E$\otimes$e Jahn—Teller potential energy surface perturbed by low-symmetry terms. An analysis of the anisotropic displacement parameters from the X-ray results shows a clear relationship to the bond length distances which is consistent with these being due to averaging. The EXAFS experiments provide the first direct data on the local geometry of the Cu(D$_2$O)$_6^{2+}$ ion at high temperature in the compound and clearly demonstrate the validity of the models previously used to interpret its behavior.

Supporting Information Available: Details of the vibronic calculations and the derivation of the displacement amplitudes ΔU_{obs} (eq 7) in PDF format. This material is available free of charge via the Internet at http://pubs.acs.org.

(26) Sham, T. K.; Hastings, B. J.; Perlman, M. L. *Chem. Phys. Lett.* **1981**, *83*, 391–396.

(27) Beagley, B.; Eriksson, A.; Lindgren, J.; Persson, I., M., P. L. G., Sandström, M., Wahlgren, U. and White, E. W. *J. Phys.*: *Condens. Matter* **1989**, *1*, 2395–2408.

(28) Figgis, B. N.; Sobolev, A. N.; Simmons, C. J.; Hitchman, M. A. Stratemeier, H.; Riley, M. J. *Acta Crystallogr.* **2000**, *B56*, 438–443.

(29) Figgis, B. N.; Iverson, B. B.; Larsen, F. K. Reynolds, P. A. *Acta Crystallogr. B* **1993**, *49*, 794–806.

(30) Figgis, B. N.; Khor, L.; Kucharski, E. S.; Reynolds, P. A. *Acta Crystallogr. B* **1992**, *48*, 144–151.

(31) Iversen, B. B.; Larsen, F. K.; Reynolds, P. A.; Figgis, B. N. *Acta Chem. Scand.* **1994**, *48*, 800–809.